1993ApJ...417....3P

THE ASTROPHYSICAL JOURNAL, 417:3–11, 1993 November 1
© 1993. The American Astronomical Society. All rights reserved. Printed in U.S.A.

ASPECTS OF ZEL'DOVICH APPROXIMATION

T. PADMANABHAN
Inter-University Centre for Astronomy and Astrophysics, Poona University Campus, Ganeshkhind, Pune 411 007, India;
e-mail: paddy@iucaa.ernet.in

AND

K. SUBRAMANIAN
National Centre for Radio Astrophysics, TIFR, Poona University Campus, Ganeshkhind, Pune 411, 007, India;
e-mail: kandu@gmrt.ernet.in

Received 1992 July 23; accepted 1993 April 15

ABSTRACT

A generalized version of the Zel'dovich approximation which is applicable in both the radiation-dominated and the matter-dominated epochs is presented. This approximation allows one to follow the growth of inhomogeneities from the time the mode enters the Hubble radius until it turns around. Comparison of the results with the standard spherical model shows that the analytic approximation is quite good even in the nonlinear regime. Detailed application to cold dark matter models and seeded models are given.

Subject headings: early universe — large-scale structure of universe

1. INTRODUCTION

It is generally believed that galaxies and other large-scale structures in the universe have formed by the enhancement of density fluctuations through gravitational instability. The spherical top-hat model (Peebles 1980) and the Zel'dovich approximation (Zel'dovich 1970) are two useful procedures to describe analytically the late stages of such an evolution, when the density inhomogeneity is no longer small. The spherical model and the Zel'dovich approximation are usually used in literature when the following conditions are satisfied: (*a*) the length scales of interest are small compared with the Hubble radius, thereby allowing the use of Newtonian approximation, and (*b*) the background density of the universe is dominated by nonrelativistic matter. As we shall discuss in this paper, the second assumption is not necessary for the validity of these two approximations. In particular, we explicitly demonstrate how to do calculations using the spherical model and the Zel'dovich approximation, starting out from the radiation-dominated era itself. This is especially relevant for fluctuations in the scale of galaxies and clusters which enter the Hubble radius in the radiation-dominated era. The amplitude of the fluctuation on any scale is most naturally specified when that scale enters the Hubble radius. The usual procedure is to follow the evolution of these perturbations using linear perturbation theory until well after the epoch of matter domination, and then use these results to set initial conditions for calculations following the nonlinear evolution. This two-step approach may not be required if one follows the methods set out in this paper, which is also especially convenient in making analytical estimates.

The plan of the paper is as follows: In §§ 2 and 3 we generalize the Zel'dovich approximation and the spherical model, so that they can be used right from the radiation-dominated era. The application of our results to some concrete models of structure formation are given in § 4.

2. THE GENERALIZED ZEL'DOVICH APPROXIMATION

We will assume throughout that the size of any inhomogeneous region of interest is much smaller than the Hubble radius, $d_H = (\dot{a}/a)^{-1}$, where $a(t)$ is the scale factor of the background Friedmann universe. In this case we can study the dynamics of this region using the Newtonian approximation. In the Newtonian limit the geometry of the Friedmann universe can be completely described by an equivalent Newtonian gravitational potential:

$$\phi_b = -\frac{1}{2}\left(\frac{\ddot{a}}{a}\right)r^2 . \tag{1}$$

Here $r = a(t)|\boldsymbol{x}|$ is the proper radial coordinate, and $\boldsymbol{x}$ is the comoving Friedmann coordinate. It may be noted that the Newtonian approximation does not require any constraints to be placed on the stress tensor of the matter. In particular, equation (1) applies equally well to the radiation-dominated era with the scale factor being governed by the Einstein equations:

$$\frac{\ddot{a}}{a} = -\frac{4\pi G}{3}(\rho_b + 3p_b) , \quad \left(\frac{\dot{a}}{a}\right)^2 = \frac{8\pi G}{3}\rho_b , \tag{2}$$

where ρ_b and p_b are the density and pressure of the background universe which is assumed to have $\Omega = 1$. In this work we will take $\rho_b(t) = \rho_m(t) + \rho_r(t)$ and $p_b(t) = \rho_r/3$, where ρ_m and ρ_r are the background densities of nonrelativistic matter and relativistic matter ("radiation"), respectively. (We have also set $c = 1$.)

Now consider an inhomogeneous region where the matter density differs from the background value. We will assume that only the nonrelativistic, matter component of the density is perturbed, and the radiation is not. The dynamics of the inhomogeneity is then determined by the perturbed gravitational potential,

$$\phi_{\rm total}(\boldsymbol{r}, t) = \phi_b(\boldsymbol{r}, t) + \delta\phi(\boldsymbol{r}, t) = -\frac{1}{2}\left(\frac{\ddot{a}}{a}\right)r^2 + \delta\phi(\boldsymbol{r}, t) , \tag{3}$$

where $\delta\phi$ is the potential generated by the excess matter density via

$$\nabla^2\delta\phi = 4\pi G(\rho - \rho_m) . \tag{4}$$

© American Astronomical Society • Provided by the NASA Astrophysics Data System

1993ApJ...417....3P

The motion of a particle in the perturbed gravitational potential $\phi_{\rm total} = \phi_b + \delta\phi$ (where ϕ_b is given by eq. [1] and $\delta\phi$ is determined by eq. [4]) is determined by the equation

$$\frac{d^2\boldsymbol{r}}{dt^2} = -\nabla\phi_{\rm total} = \left(\frac{\ddot{a}}{a}\right)\boldsymbol{r} - \nabla\delta\phi \ . \tag{5}$$

We know that in the absence of the perturbation $\boldsymbol{r} = a(t)\boldsymbol{q}$ will solve equation (5), with any constant $\boldsymbol{q}$. We shall, therefore attempt to solve equation (5) approximately by the Zel'dovich *Ansatz*

$$\boldsymbol{r}(t) = a(t)[\boldsymbol{q} + \boldsymbol{f}(\boldsymbol{q}, t)] \equiv a(t)\boldsymbol{x} \ , \tag{6}$$

where we shall treat $\boldsymbol{f}$ as a perturbation on $\boldsymbol{q}$. Here $\boldsymbol{q}$ can be thought of as the Lagrangian coordinate of a particle, and $\boldsymbol{x}$ is the comoving Eulerian coordinate of the particle whose Lagrangian position is $\boldsymbol{q}$. In general, equation (6) gives a coordinate transformation between the $\boldsymbol{q}$ and the $\boldsymbol{r}$ (or $\boldsymbol{x}$) space, provided that the transformation is invertible. We shall often use equation (6) in this sense below. Substituting equation (6) in equation (5), we get

$$a^2\ddot{\boldsymbol{f}} + 2a\dot{a}\dot{\boldsymbol{f}} = -a\nabla_{\boldsymbol{r}}\delta\phi = -\nabla_{\boldsymbol{x}}\delta\phi \ , \tag{7}$$

where, in the last step, we have changed the coordinates from $\boldsymbol{r}$ to $\boldsymbol{x}$. Solutions can now be found by taking the divergence or curl of equation (7) with respect to the $\boldsymbol{x}$-coordinate. Note that derivatives with respect to $\boldsymbol{x}$ can be converted to derivatives with respect to $\boldsymbol{q}$ using equation (6).

Taking the divergence of all the terms in equation (7), and using the Poisson's equation (4), we get

$$\nabla_{\boldsymbol{x}} \cdot [a^2\ddot{\boldsymbol{f}} + 2a\dot{a}\dot{\boldsymbol{f}}] = -\nabla_{\boldsymbol{x}}^2\delta\phi = -4\pi G a^2(\rho - \rho_m) \ . \tag{8}$$

We shall try to separate the t and $\boldsymbol{q}$ dependence in this equation by writing

$$\boldsymbol{f}(\boldsymbol{q}, t) = b(t)\boldsymbol{p}(\boldsymbol{q}) \ . \tag{9}$$

Note that such a separation is certainly valid in the linear regime and is the usual *Ansatz* invoked in the Zel'dovich approximation. Using equation (9), equation (8) becomes

$$\left(\ddot{b} + \frac{2\dot{a}}{a}\dot{b}\right)\frac{\partial q^j}{\partial x^i}\frac{\partial p^i}{\partial q^j} = -4\pi G(\rho - \rho_m) \ . \tag{10}$$

The right-hand side of equation (10) can be rewritten using the equation for mass conservation. We have, for the perturbed density, the relation

$$\rho(\boldsymbol{r}, t)d^3\boldsymbol{r} = \rho_i(\boldsymbol{q})d^3\boldsymbol{q}\, a_i^3 \ , \tag{11}$$

where $\rho_i(\boldsymbol{q})$ is the initial density field. [In general, $\rho_i(\boldsymbol{q})$ may differ from the background matter density, $\rho_m(t_i)$, at the initial time t_i. We have also assumed that at a sufficiently early initial time t_i, $\boldsymbol{f}(\boldsymbol{q}, t_i) = 0$.] So

$$\rho(\boldsymbol{r}, t) = \rho_i(\boldsymbol{q})a_i^3 \det\left(\frac{\partial q^i}{\partial r^j}\right) = \frac{\rho_i(\boldsymbol{q})(a_i^3/a^3)}{\det\,[\delta_{ij} + b(t)(\partial p^j/\partial q^i)]} \equiv \frac{\rho_i(\boldsymbol{q})(a_i^3/a^3)}{D} \ , \tag{12}$$

where we have defined $D \equiv \det\,[\delta_{ij} + b(t)(\partial p^j/\partial q^i)]$. Using equation (12) in equation (10), we then have

$$\left(\ddot{b} + \frac{2\dot{a}}{a}\dot{b}\right)\frac{\partial q^j}{\partial x^i}\frac{\partial p^i}{\partial q^j} = -4\pi G\rho_m(t)\,\frac{[(\rho_i(q)/\rho_m(t_i)) - D]}{D} \ . \tag{13}$$

The discussion was exact so far. We shall now introduce the small-$\boldsymbol{f}$ approximation. For small $\boldsymbol{f}$, we need to retain only terms that are linear in $b\boldsymbol{p}$ in equation (13). From equation (6) we have

$$\frac{\partial p^i}{\partial q^j} = \frac{\partial p^i}{\partial x^k}\frac{\partial x^k}{\partial q^j} = \left(\delta_{kj} + b\frac{\partial p^k}{\partial q^j}\right)\frac{\partial p^i}{\partial x^k} \approx \frac{\partial p^i}{\partial x^j} + O(bp) \ . \tag{14}$$

Hence, on the left-hand side of equation (13), to the leading order, we can replace $\nabla_{\boldsymbol{x}} \cdot \boldsymbol{p}$ by $\nabla_{\boldsymbol{q}} \cdot \boldsymbol{p}$. The determinant appearing on the right-hand side of equation (13) is $D \approx (1 + b\nabla_{\boldsymbol{q}} \cdot \boldsymbol{p}) + O(b^2p^2)$. So, to the leading order, equation (13) becomes

$$\left[\ddot{b} + \frac{2\dot{a}}{a}\dot{b} - 4\pi G\rho_m(t)\frac{\rho_i(q)}{\rho_m(t_i)}b\right]\nabla_{\boldsymbol{q}} \cdot \boldsymbol{p} = -4\pi G\rho_m(t)\left[\frac{\rho_i(q)}{\rho_m(t_i)} - 1\right] . \tag{15}$$

We see from equation (15) that we must have $[\rho_i(q)/\rho_m(t_i) - 1] \ll 1$ for our approximation to be consistent; in this case, to the leading order, we can replace $[\rho_i(q)/\rho_m(t_i)]$ on the left-hand side of equation (15) by unity. Therefore,

$$\left[\ddot{b} + \frac{2\dot{a}}{a}\dot{b} - 4\pi G\rho_m(t)b\right]\nabla_{\boldsymbol{q}} \cdot \boldsymbol{p} = -4\pi G\rho_m(t)\left[\frac{\rho_i(q)}{\rho_m(t_i)} - 1\right] . \tag{16}$$

It is now convenient to split $\boldsymbol{p}$ into a curl-free (longitudinal) part $\boldsymbol{p}^L$ and a divergence-less (rotational) part $\boldsymbol{p}^R$:

$$\boldsymbol{p}(\boldsymbol{q}) = \boldsymbol{p}^L(\boldsymbol{q}) + \boldsymbol{p}^R(\boldsymbol{q}); \quad \nabla_{\boldsymbol{q}} \cdot \boldsymbol{p}^R = 0 = \nabla_{\boldsymbol{q}} \times \boldsymbol{p}^L \ . \tag{17}$$

Only the $\boldsymbol{p}^L$ part survives in equation (16). The solution to the linear, inhomogeneous differential equation (16) can be written as the sum of a particular solution which satisfies equation (16) and a homogeneous part, say $b_H\boldsymbol{p}_H^L$, (with an arbitrary $\boldsymbol{p}_H^L$), which satisfies equation (16) with its right-hand side set to zero. Thus we can write $\boldsymbol{f} = b_H\boldsymbol{p}_H^L + b_P\boldsymbol{P}$, where b_H satisfies the equation

$$\ddot{b}_H + \frac{2\dot{a}}{a}\dot{b}_H - 4\pi G\rho_m(t)b_H = 0 \ , \tag{18}$$

and $b_P\boldsymbol{P}$ is a particular solution of equation (16). (Note that $\boldsymbol{P}$ is also curl-free, since by definition it is the difference between $\boldsymbol{p}^L$ and $\boldsymbol{p}_H^L$). One particular solution can be easily obtained by the following procedure: If we choose

$$\nabla_{\boldsymbol{q}} \cdot \boldsymbol{P}(\boldsymbol{q}) = \left[\frac{\rho_i(q)}{\rho_m(t_i)} - 1\right] , \tag{19}$$

and define a new variable $B_P = b_P - 1$, then B_P satisfies exactly the same equation (eq. [18]) as b_H. *So the only nontrivial equation which needs to be solved to obtain the time dependence of the longitudinal part of* $\boldsymbol{f}$ *is equation* (18).

This equation is well known in the literature. It can be recast in the form

$$2y(1 + y)g'' + (2 + 3y)g' - 3g = 0 \ , \tag{20}$$

where g can be b_H or B_P; $y = a(t)/a_{\rm eq}$, where $a_{\rm eq}$ is the scale factor of the universe when matter and radiation densities are equal and the prime denotes differentiation with respect to y. This is the standard equation governing the growth of linear density perturbations. (We will encounter this equation again

© American Astronomical Society • Provided by the NASA Astrophysics Data System

1993ApJ...417....3P

in the next section.) It has two general solutions, $D_1(y)$ and $D_2(y)$, with (see Peebles 1980, eqs. [12.4], [12.5], and [12.9]):

$$D_1(y) = 1 + \tfrac{3}{2}y\,, \tag{21}$$

$$D_2(y) = \left(1 + \frac{3}{2}y\right)\ln\left[\frac{(1+y)^{1/2}+1}{(1+y)^{1/2}-1}\right] - 3(1+y)^{1/2}\,. \tag{22}$$

Gathering together all the pieces, we can express the longitudinal part $\boldsymbol{f}^L$ of $\boldsymbol{f}$ as

$$\boldsymbol{f}^L(q,\,t) = c_1\,D_1(t)\boldsymbol{p}_1^L(\boldsymbol{q}) + c_2\,D_2(t)\boldsymbol{p}_2^L(\boldsymbol{q}) + [c_3\,D_1(t) + c_4\,D_2(t) + 1]\boldsymbol{P}(\boldsymbol{q})\,, \tag{23}$$

where $\boldsymbol{p}_1^L$ and $\boldsymbol{p}_2^L$ are arbitrary curl-free vector fields.

Let us now return to equation (7) and take the curl of all its terms. We get

$$\nabla_{\boldsymbol{x}} \times (a^2\ddot{\boldsymbol{f}} + 2a\dot{a}\dot{\boldsymbol{f}}) = 0\,. \tag{24}$$

Once again separating the $\boldsymbol{q}$ and t dependence and changing from the $\boldsymbol{x}$ to $\boldsymbol{q}$ coordinates, equation (24) becomes

$$\epsilon_{ijk}\frac{\partial q^l}{\partial x^j}\frac{\partial p^k}{\partial q^l}(a^2\ddot{b} + 2a\dot{a}\dot{b}) = 0\,. \tag{25}$$

Using equation (14), we can replace, to the leading order, $(\nabla_{\boldsymbol{x}} \times \boldsymbol{p})$ in the above equation by $(\nabla_{\boldsymbol{q}} \times \boldsymbol{p})$. Then only the rotational part of $\boldsymbol{p}$ survives in the above equation. Also from equation (25), we see that the corresponding $b(t) = b_R(t)$ satisfies

$$\ddot{b}_R + 2\frac{\dot{a}}{a}\dot{b}_R = 0\,, \tag{26}$$

which has a general solution

$$b_R(t) = k_1\int^t \frac{dt}{a^2} + k_2\,. \tag{27}$$

So we have for the rotational part of $\boldsymbol{f} = \boldsymbol{f}^R$ the solution

$$\boldsymbol{f}^R(\boldsymbol{q},\,t) = \boldsymbol{p}_1^R(\boldsymbol{q})\int^t \frac{dt}{a^2} + \boldsymbol{p}_2^R(\boldsymbol{q})\,, \tag{28}$$

where $\boldsymbol{p}_1^R$ and $\boldsymbol{p}_2^R$ are arbitrary divergence-free vector fields.

Combining the rotational and longitudinal parts of $\boldsymbol{f}$ given in equations (28) and (23) and collecting the coefficients of D_1 and D_2 by redefining the $\boldsymbol{p}$'s, we finally have the general approximate solution to equation (5):

$$\boldsymbol{r}(t) = a(t)\left[\boldsymbol{q} + D_1(t)\boldsymbol{p}_{1N}^L(\boldsymbol{q}) + D_2(t)\boldsymbol{p}_{2N}^L(\boldsymbol{q}) + \boldsymbol{P}(\boldsymbol{q}) + \boldsymbol{p}_1^R(\boldsymbol{q})\int^t \frac{dt}{a^2} + \boldsymbol{p}_2^R(\boldsymbol{q})\right], \tag{29}$$

where $\boldsymbol{p}_{1N}^L = c_1\boldsymbol{p}_1^L + c_3\boldsymbol{P}$ and $\boldsymbol{p}_{2N}^L = c_2\boldsymbol{p}_2^L + c_4\boldsymbol{P}$. *This is a generalization of the Zel'dovich approximation applicable to the radiation-dominated era as well.* In the special case of a matter-dominated universe, equation (29) goes over into the vortical pancake solution discussed by Buchert (1992; also see Buchert 1989).

The functions $\boldsymbol{p}(\boldsymbol{q})$ in equation (29) can be fixed from the initial conditions. These can be taken to be the initial density field $\rho_i(\boldsymbol{q})$ defined earlier and the initial peculiar velocity field, say $\boldsymbol{u}(\boldsymbol{q},\,t_i) \equiv \dot{\boldsymbol{r}} - (\dot{a}/a)\boldsymbol{r}$. We again split up $\boldsymbol{u}$ into a longitudinal part $\boldsymbol{U}^L$ and a transverse part $\boldsymbol{U}^R$. Imposing the initial conditions

$$\boldsymbol{f}(q,\,t_i) = 0;\quad \boldsymbol{u}(\boldsymbol{q},\,t_i) = \boldsymbol{U}^L(\boldsymbol{q}) + \boldsymbol{U}^R(\boldsymbol{q})\,, \tag{30}$$

we then get

$$\boldsymbol{r}(t) = a(t)\left[\boldsymbol{q} + \boldsymbol{P}\left(1 + y_i(1+y_i)^{1/2}\frac{db_e}{dy_i}(y,\,y_i)\right) + \frac{\boldsymbol{U}^L}{H_i a_i}b_e(y,\,y_i)(1+y_i)^{1/2} + \frac{\boldsymbol{U}^R}{a_i}\int_{t_i}^t dt\left(\frac{a_i}{a}\right)^2\right], \tag{31}$$

where

$$b_e(y,\,y_i) = D_1(y)D_2(y_i) - D_2(y)D_1(y_i)\,;$$

$$\frac{db_e}{dy_i}(y,\,y_i) = D_1(y)\frac{dD_2}{dy}(y_i) - D_2(y)\frac{dD_1}{dy}(y_i)\,, \tag{32}$$

and $\boldsymbol{P}$ is determined by equation (19) as before.

3. THE GENERALIZED SPHERICAL MODEL

We shall now generalize the spherical model to the radiation-dominated era (also see Mészáros 1975) and also show that the nonlinear aspects of density growth are very well approximated by the Zel'dovich approximation described above.

3.1. *Mathematical Formulation*

Consider a situation in which the initial inhomogeneity was spherically symmetric about some origin. The dynamics of this region is again determined by the potential $\phi_{\rm total} = \phi_b + \delta\phi$, where $\delta\phi$ is now spherically symmetric. The motion of a thin spherical shell of particles is governed by the equation

$$\frac{d^2\boldsymbol{r}}{dt^2} = -\nabla\phi_{\rm total} = \left(\frac{\ddot{a}}{a}\right)\boldsymbol{r} - \frac{G\,\delta M}{r^3}\boldsymbol{r}\,. \tag{33}$$

Here δM is the excess mass of nonrelativistic matter contained within the shell, over and above the mass contributed by the background universe $M_{\rm bm} = (4\pi\rho_m(t)r^3/3)$. Using equation (2) for $a(t)$, we can rewrite equation (33) as

$$\frac{d^2r}{dt^2} = -\frac{4\pi}{3}G(2\rho_r + \rho_m)r - \frac{G\,\delta M}{r^2} = -\frac{8\pi G}{3}\rho_r(t)r - \frac{GM}{r^2}\,. \tag{34}$$

In the above $r \equiv |\boldsymbol{r}|$ and $M = M_{\rm bm} + \delta M$ is the total nonrelativistic mass enclosed in the shell radius r. In many practical applications one can assume that the shells at different radii do not cross each other during most of their evolution. In this case M in equation (34) is constant in time.

The evolution described by equation (34) reduces to the usual spherical model (discussed, for example, in Peebles 1980, § 19), when $\rho_r \ll \rho_m$, that is, when the universe is matter-dominated. On the other hand, in the radiation-dominated era with $\rho_r \gg \rho_m$, one cannot neglect the extra term which is proportional to $\rho_r(t)r$, and equation (34) provides a nonlinear generalization of what is known as the "stagspansion phase" in the linear theory of growth of perturbations. To solve equation (34) and to understand its implications, it is convenient to change to a new independent variable $y = (a/a_{\rm eq})$ and a new dependent variable $x = (r/a(t))$; as before, $a_{\rm eq}$ denotes the value of the scale factor at the time $t_{\rm eq}$ when the densities of radiation

© American Astronomical Society • Provided by the NASA Astrophysics Data System

1993ApJ...417....3P

and matter were equal. Einstein equations (2) can be rewritten in the form

$$\frac{\ddot{y}}{y} = -\frac{1}{\tau_{eq}^2}\left(\frac{1}{y^4}+\frac{1}{2y^3}\right); \quad \left(\frac{\dot{y}}{y}\right)^2 = \frac{1}{\tau_{eq}^2}\left(\frac{1}{y^4}+\frac{1}{y^3}\right). \quad (35)$$

Here we have used the fact that $\rho_m = \rho_{eq}\, y^{-3}$ and $\rho_r = \rho_{eq}\, y^{-4}$, where ρ_{eq} is the matter (or radiation) density at t_{eq}, and $\tau_{eq} = (8\pi G\rho_{eq}/3)^{-1/2}$. (Note that the total density at $t = t_{eq}$ is $2\rho_{eq}$.) Using equation (35) and making the above change of coordinates, we transform equation (34) to the equation

$$2y(1+y)\frac{d^2x}{dy^2} + (2+3y)\frac{dx}{dy} - x + \left(\frac{2GM\tau_{eq}^2}{a_{eq}^3}\right)\frac{1}{x^2} = 0. \quad (36)$$

This equation can be converted into a more convenient form by using the dimensionless variable

$$l \equiv \frac{x}{x_c}; \quad x_c = \left(\frac{2GM\tau_{eq}^2}{a_{eq}^3}\right)^{1/3}. \quad (37)$$

Then we get

$$2y(y+1)\frac{d^2l}{dy^2} + (2+3y)\frac{dl}{dy} - l + \frac{1}{l^2} = 0. \quad (38)$$

This is the basic nonlinear equation which we have to solve in order to follow the evolution of a spherical shell which has entered the Hubble radius in the radiation-dominated era. This equation, as far as we know, does not have a closed analytic solution. We shall now solve it approximately using the Zel'dovich-type approximation described in the last section and compare it with exact numerical solution.

3.2. *Approximate Analytic Solution*

To begin with, we note that one obvious solution to equation (36) is $x = x_c$ or, equivalently, $l = 1$. In the absence of perturbation the total mass enclosed in the shell is just the mass due to the background density: $M = M_{bm}$. In this case, it is easy to verify that $x_c = (r_{eq}/a_{eq})$. That is, x_c is the comoving radius of a sphere in a FRW universe containing the mass M_b. Then $r(t) = (a(t)r_{eq}/a_{eq})$, and this solution represents the unperturbed Hubble expansion of the shell. In the presence of an initial mass perturbation x_c is no longer the unperturbed comoving radius. But the unperturbed case suggests that we can look for an approximate solution to equation (36) in terms of a perturbed trajectory of the shell $l(t) = 1 + f(t)$ with $f(t) \ll 1$. This is completely analogous to the Zel'dovich approximation in which one follows the nonlinear evolution of density contrasts, using a linearization of the particle trajectories. Substituting the above *Ansatz* in equation (36) and retaining only terms linear in $f(y)$, we get

$$2y(1+y)\frac{d^2f}{dy^2} + (2+3y)\frac{df}{dy} - 3f = 0. \quad (39)$$

Equation (39) is identical to equation (12.4) in Peebles (1980) and equation (20) in the last section. It has two general solutions, $D_1(y)$ and $D_2(y)$, given by equations (21) and (22). So we can write the approximate solution in the form $f = \bar{A}D_1 + \bar{B}D_2$; this implies that $r = ax = ax_c\, l = ax_c(1+f)$:

$$r(t) = a(t)[x_c + AD_1(a(t)) + BD_2(a(t))], \quad (40)$$

with new constants $A = x_c\,\bar{A}$, $B = x_c\,\bar{B}$. These constants are determined by the initial values $f_i = f(y_i)$ and $f_i' = f'(y_i)$. Equivalently, we can specify the initial radius $r_i = r(t_i)$ and the initial peculiar velocity $v_i(r_i)$ of each shell. Here the initial peculiar velocity of the shell is defined through the equation

$$\left(\frac{dr}{dt}\right)_i = \left(\frac{\dot{a}}{a}\right)_i r_i + v_i \equiv H_i r_i + v_i. \quad (41)$$

Direct calculation gives

$$A = -y_i(1+y_i)^{1/2}\left[D_2'(y_i)x_c(l_i-1) - D_2(y_i)H_i^{-1}\left(\frac{v_i}{a_{eq}\,y_i^2}\right)\right], \quad (42)$$

$$B = -y_i(1+y_i)^{1/2}\left[-D_1'(y_i)x_c(l_i-1) + D_1(y_i)H_i^{-1}\left(\frac{v_i}{a_{eq}\,y_i^2}\right)\right], \quad (43)$$

where $l_i = r_i/(a_i x_c)$. Note that the initial density within the sphere is determined by f_i, or, equivalently, by l_i. We have

$$\rho_i = \frac{3M}{4\pi r_i^3} = \frac{3M}{4\pi a_i^3 (x_c\, l_i)^3}; \quad \rho_b = \frac{3M}{4\pi a_i^3\, x_c^3}, \quad (44)$$

so that

$$\left(\frac{\rho_i}{\rho_b}\right) \equiv \alpha^3 = \frac{1}{l_i^3}. \quad (45)$$

The initial density contrast is

$$\delta_i = \frac{\rho_i - \rho_b}{\rho_b} = \left(\frac{1}{l_i^3} - 1\right), \quad (46)$$

giving $l_i = (1+\delta_i)^{-1/3}$ and $\alpha = (1+\delta_i)^{1/3}$. This form of the solution is convenient for numerical computations. The solution can also be expressed, in terms of δ_i and v_i, in a form convenient for making analytical estimates. Substituting A and B in equation (40) and using the definition of l_i, we get

$$r(t) = \frac{a(t)}{a_i}\left[\alpha r_i - (1-\alpha)r_i\, y_i(1+y_i)^{1/2}\frac{db_e}{dy_i}(y, y_i) + \frac{v_i(1+y_i)^{1/2}}{H_i}\, b_e(y, y_i)\right], \quad (47)$$

where $b_e(y, y_i)$ and (db_e/dy_i) are as defined in equation (32).

One can, in fact, improve the validity of the Zel'dovich-type approximate solution to equation (38) by doing higher order perturbation theory. But if the analytic solution obtained by such a process is too cumbersome to handle, one loses the motivation for including the higher orders. It turns out, however, that the approximate analytic solution to the second order in f is still sufficiently simple that it is worth pointing out. Suppose we write $l = 1 + f_1 + f_2$, where $f_1 \ll 1$ and $f_2 \ll f_1$. Then f_1 satisfies equation (39) as before, while for f_2 we get the next order equation:

$$2y(1+y)\frac{d^2f_2}{dy^2} + (2+3y)\frac{df_2}{dy} - 3f_2 = -3f_1^2. \quad (48)$$

For sufficiently small initial perturbations, f_2 will become important only at late times: $y \gg 1$. So when substituting for f_1 on the right-hand side of equation (48), one can neglect the "decaying" solution $\bar{B}D_2$ in equation (40). Also, to the same order of accuracy, we can ignore the corrections to the constants A and B due to f_2 and determine them as before: the

© American Astronomical Society • Provided by the NASA Astrophysics Data System

1993ApJ...417....3P

above equation for f_2 then becomes

$$2y^2 \frac{d^2 f_2}{dy^2} + 3y \frac{df_2}{dy} - 3f_2 = -3\bar{A}^2 D_1^2 = -\frac{27}{4} \bar{A}^2 y^2 , \quad (49)$$

which has a power-law solution of the form $f_2 = -(27/28)\bar{A}^2 y^2$. So, to the second order, we have

$$r(t) = a(t)\left[x_c + AD_1(y) + BD_2(y) - \frac{27A^2}{28x_c} y^2 \right], \quad (50)$$

with A and B given as in equations (42) and (43) above.

Notice that the approximation used in arriving at equation (39) from equation (38) involves the assumption $f \ll 1$. If this is true, then the density contrast $\delta(y)$ at any time will be

$$\delta = \frac{1}{l^3} - 1 \cong (1+f)^{-3} - 1 = -3f . \quad (51)$$

Thus, as long as $\delta \ll 1$, δ and f satisfy the same equations. This is the standard, well-known result in the linear theory of perturbations. Consider now the nonlinear regime when the condition $\delta \ll 1$ is *not* satisfied. One can handle this situation using the spherical model. In that case

$$\delta_{SM} = \frac{1}{l_{SM}^3} - 1 , \quad (52)$$

where l_{SM} is the solution to the *exact* equation (38). The crucial point, however, is the following: we shall show that δ_{SM} is very well approximated by

$$\delta_Z = \frac{1}{l_Z^3} - 1 , \quad (53)$$

where l_Z is the *approximate* solution discussed above. In other words, our approximation to the trajectories allows one to compute *nonlinear* densities; what is more, the approximation works even in the radiation-dominated phase. In a way, we get "nonlinear results for linear effort."

TABLE 1

PARAMETERS AT TURNAROUND

a_i/a_{eq}	x_i (Mpc)	r_t(exact) (Mpc)	r_t(approx) (Mpc)	y_t(exact)	y_t(approx)
0.03.....	0.236	0.193	0.197	8.65×10^3	8.65×10^3
1.00.....	6.55	17.4	18.6	2.5×10^4	3.16×10^4

3.3. *Numerical Integration*

To demonstrate the above claim, we need to integrate equation (38) and compare the solution with the one in equation (40). This is done in Figures 1 and 2.

Figures 1*a* and 1*b* show the behavior of the shell radius r as a function of the expansion factor $y = (a/a_{eq})$ in a universe with $\Omega = 1$, $h = 0.5$. The dashed lines correspond to the Zel'dovich approximation, while the solid line is the exact solution. Figure 1*a* has $y_i = 0.03$, and Figure 1*b* has $y_i = 1$. The comoving radius x_c of the shell is taken to be one-tenth of the horizon size at y_i in both cases. (This gives $x_c = 0.236$ Mpc for $y_i = 0.03$ and $x_c = 6.55$ Mpc for $y_i = 1$.) In both cases we have taken an initial density contrast of $\delta_i = 10^{-4}$ and set $v_i = 0$. The general pattern of the results does not depend sensitively on these parameters.

The line with short dashes denotes the first-order approximation, while the one with long dashes (closer to the exact curve) denotes the approximation correct to second order. It is clear that our approximation tracks the exact solution fairly well and that adding the second-order corrections improves the situation considerably. (In order to highlight the *difference* between the exact and approximate solutions, we have used a linear scale on the y-axis and a logarithmic scale on the x-axis!) The parameters at turnaround are given in Table 1,

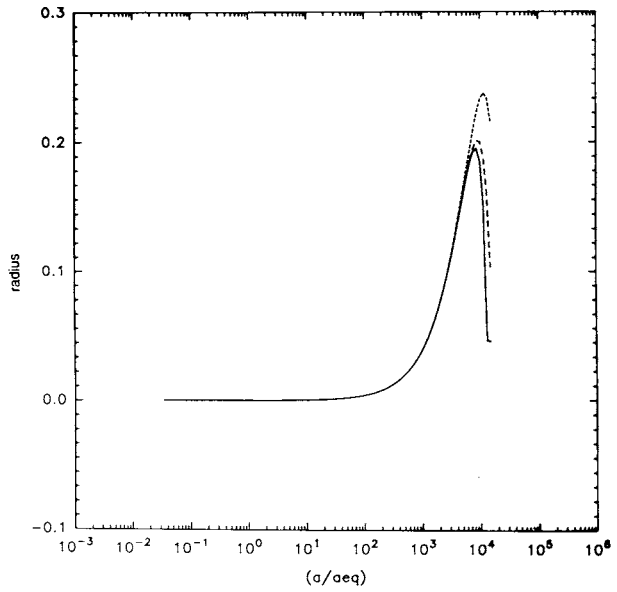

FIG. 1*a*

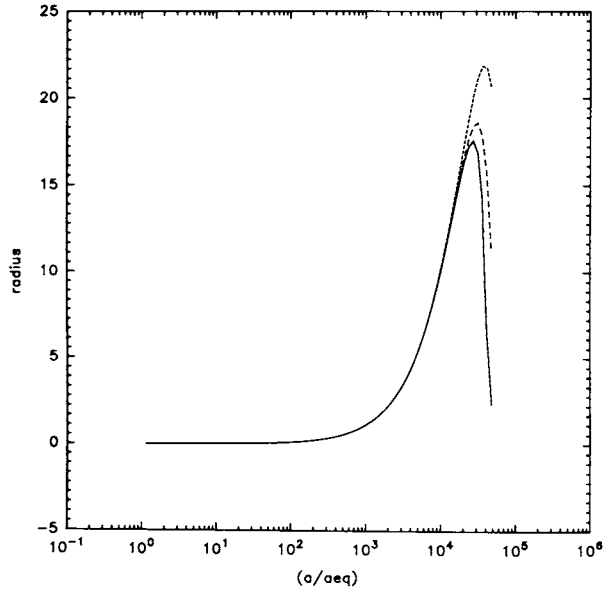

FIG. 1*b*

FIG. 1.—Radius of the overdense shell as a function of the expansion factor. The solid line is obtained from the exact numerical integration of the equation; the short-dashed line is the first-order approximation, and the long-dashed line (which is closer to the exact solution) is the second-order correction. We have taken $h = 0.5$, $\Omega = 1$, and $\delta_i = 10^{-4}$. (*a*) $y_i = 0.03$; (*b*) $y_i = 1$.

© American Astronomical Society • Provided by the NASA Astrophysics Data System

1993ApJ...417....3P

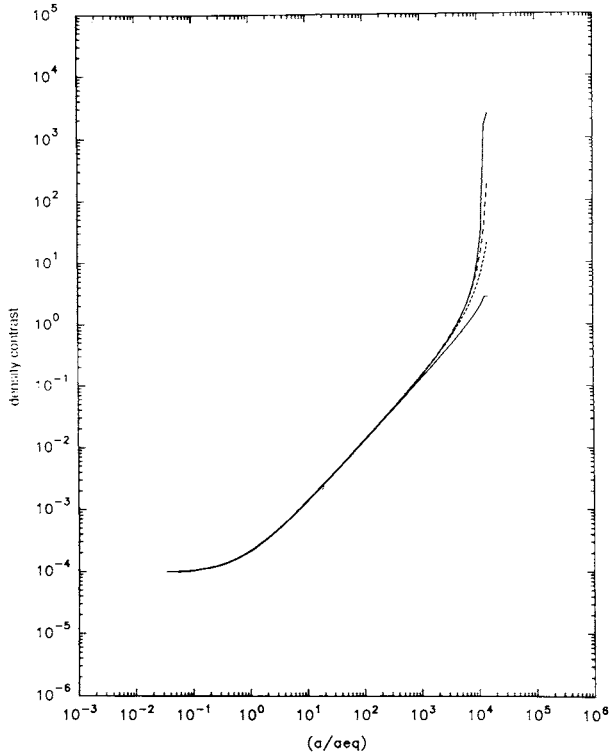

FIG. 2a

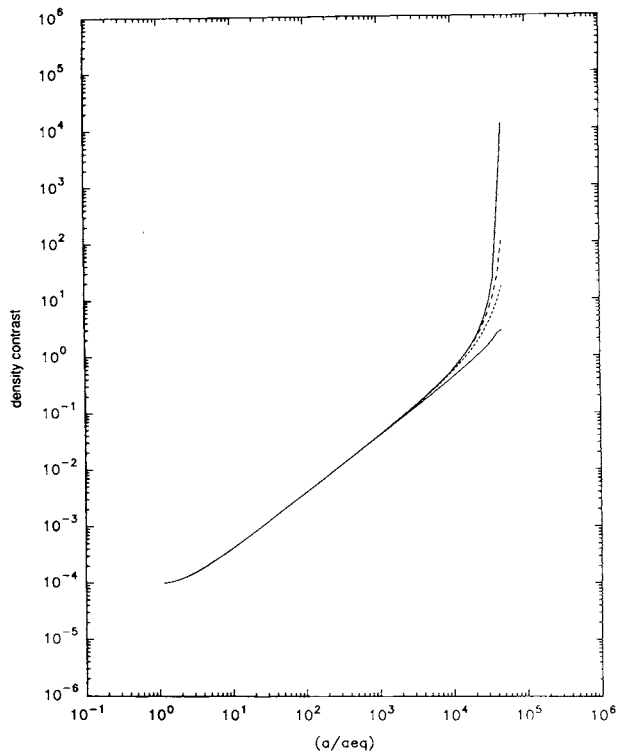

FIG. 2b

FIG. 2.—Density contrast of the overdense shell as a function of the expansion factor. The top solid curve is from numerical integration of the equation while the bottom solid curve is the result of linear theory. The short-dashed and long-dashed curves are the analytic approximations with first- and second-order corrections, respectively. We have taken $h = 0.5, \Omega = 1$, and $\delta_i = 10^{-4}$. (*a*) $y_i = 0.03$; (*b*) $y_i = 1$.

which shows that the approximation is reasonably accurate even when the sphere has reached its maximum radius.

To illustrate these points further, Figures 2*a* and 2*b* show the evolution of the density contrast as a function of the scale factor, for the parameters of Figures 1*a* and 1*b*, respectively. The solid line shows the nonlinear density contrast δ_{SM} calculated using the exact solution; the short-dashed line is δ_{Z1} calculated by the first-order Zel'dovich approximation, the long-dashed line is δ_{Z2} calculated using the second-order correction, and the dotted line at the bottom is the result using linear theory. Table 2 summarizes the values corresponding to $y_i = 0.03$, $\delta_i = 10^{-4}$. It is clear from the table and the figure that the Zel'dovich approximation tracks the exact result even in the nonlinear region. For example, when $\delta_{SM} \simeq 9.7$, $\delta_Z \simeq 7.5$, off only by 30% (while, note for comparison, $\delta_{lin} \simeq 1.6$); and even when $\delta_{SM} \simeq 29$, $\delta_Z \simeq 14.4$, off only by a factor of 2 (while $\delta_{lin} \simeq 2$, off by a factor of 15).

4. APPLICATIONS AND DISCUSSION

We now apply the results of the previous section to the problem of determining the characteristic redshifts at which different mass scales go nonlinear. We will illustrate our results mainly in the context of the cold dark matter model and will briefly comment on how it can be used in seeded theories of galaxy formation like the one based on textures.

TABLE 2

EVOLUTION OF THE DENSITY CONTRAST

y	δ_{SM}	δ_Z	δ_{lin}
8.3×10^2.....	0.11	0.11	0.11
5.0×10^3.....	1.2	1.2	0.69
9.9×10^3.....	9.7	7.6	1.6
1.1×10^4.....	29.0	14.4	2.0

We will adopt the convention of defining the redshift z_{NL} at which a given mass scale goes nonlinear to be the epoch when a spherical shell enclosing that mass turns around; that is when $\dot{r} = 0$. We can estimate this epoch analytically using equation (50). In general we expect $\delta_i \ll 1$, when any given mass scale enters the Hubble radius, so that most scales are expected to turn around at $y \gg 1$. In this case, it is an excellent approximation to neglect the $BD_2(y)$ term in comparison with the $AD_1(y)$ term in equation (50) and also to take $D_1(y) \cong (3y/2)$. Using these approximations, equation (50) becomes

$$r(t) = \frac{a(t) r_i}{a_i} \left(1 - \frac{3\beta}{2} y - \frac{27}{28} \beta^2 y^2\right), \tag{54}$$

where

$$\beta = -\frac{\delta_i}{3} \frac{dD_2(y_i)}{dy} y_i (1 + y_i)^{1/2} - \frac{v_i}{H_i r_i} D_2(y_i)(1 + y_i)^{1/2}. \tag{55}$$

So the condition $\dot{r} = 0$ leads to the quadratic equation

$$1 - 3\beta y - \tfrac{81}{28} \beta^2 y^2 = 0, \tag{56}$$

whose positive root is

$$y_t = \frac{1}{\beta} \frac{14}{81} \left(\frac{12}{7^{1/2}} - 3\right) = \frac{0.2654}{\beta}. \tag{57}$$

© American Astronomical Society • Provided by the NASA Astrophysics Data System

1993ApJ...417....3P

(Note that, usually, $\beta y \ll 1$, ensuring that the second-order correction term in eq. [54] is subdominant; we see that even at turnaround $\beta y \simeq 0.26$.) Since $y = (a/a_{eq}) = [(1 + z_{eq})/(1 + z)]$, we have, for the turnaround redshift z_t,

$$(1 + z_t) = (1 + z_{eq}) y_t^{-1} = 3.768\beta(1 + z_{eq}) . \quad (58)$$

Substituting for β, we finally get

$$1 + z_t = E\left\{\delta_i(1 + z_{eq})\left[\frac{1 - (3y_i/2)(1 + y_i)^{1/2} D_2(y_i)}{1 + (3y_i/2)}\right] - \frac{3v_i}{H_i r_i}(1 + z_{eq})(1 + y_i)^{1/2} D_2(y_i)\right\} , \quad (59)$$

where

$$E = \left[\frac{14}{27}\left(\frac{12}{7^{1/2}} - 3\right)\right]^{-1} \approx 1.26 , \quad (60)$$

and we have written (dD_2/dy) in terms of D_2 using the Wronskian condition, connecting the two fundamental solutions and their derivatives. If we had retained only the first-order terms in our approximate solution, the redshift at turnaround would still have been given by equation (59), except that in this case $E = 1$. This is the reason for separating out the factor E in equation (59).

This turnaround redshift is lower than what is obtained in the standard spherical top-hat model for the same final (linear density. To obtain a relation between the two, we can proceed as follows: the *linear* density contrast based on our approximation is

$$\delta_{lin} = -3f = -3\left(\frac{r}{ax_c} - 1\right) = \frac{9}{2}\beta y . \quad (61)$$

At present $[y = y_{now} = (1 + z_{eq})]$, this has the value

$$\delta_{lin}(0) = \tfrac{9}{2}\beta(1 + z_{eq}) . \quad (62)$$

In the spherical top-hat model, we usually take the turnaround redshift to be $(1 + z_{St}) = (\delta_{lin}(0)/1.062)$ (see, for example, Peebles 1980, § 19). So we have

$$(1 + z_{St}) \cong 4.237\beta(1 + z_{eq}) . \quad (63)$$

Expressing z_{eq} in terms of z_t using equation (58) we get

$$(1 + z_{St}) \cong 1.12(1 + z_t) . \quad (64)$$

Clearly, $z_{St} > z_t$; this is to be expected because we have used a second-order approximation in equation (54), whereas the spherical model is exact in the matter-dominated phase [Incidentally, for $y_i \ll 1$, $\delta_i \ll 1$, the $(9/2)\beta y$ term in δ_{lin} has a simple interpretation. In the radiation-dominated era, δ grows by a factor of 5/2 from $y = y_i$ to $y = 1$ if $y_i \ll 1$. In the matter-dominated era $\delta = (3/5)\delta(a_{eq})y$, if $v_i \ll 1$ at $y = 1$. So $\delta(y) = (5/2)(3/5)\delta_i y = (3/2)\delta_i y$, for $y \gg 1$. Since $\beta \cong (\delta_i/3)$ for $y_i \ll 1$, $v_i = 0$, this is precisely what we get.]

To estimate z_t using equation (59) for various mass scales, one first has to specify δ_i and v_i. As an example, let us consider the cold dark matter (CDM) theory with the adiabatic scale-invariant density fluctuations. In this case δ_i for any mass scale has a Gaussian probability distribution with a variance $\sigma(M)$. For scale-invariant fluctuations, one can take σ independent of M, provided that we take the initial epoch for each mass scale to be that when the fluctuation enters the Hubble radius. In this theory we can also express v_i in terms of δ_i. To find this relation, we proceed as follows: we note that when a fluctuation is outside the Hubble radius the linear density contrast $\delta = \delta_{SH}$ grows as

$$\delta_{SH} \propto \frac{1}{(\rho_r + \rho_m)a^2} \propto \frac{y^2}{1 + y} , \quad (65)$$

where we have neglected the decaying mode (see for example Kolb & Turner 1990, p. 356; Padmanabhan 1993, p. 129). After the fluctuation has entered the Hubble radius, it initially suffers stagspansion, and its evolution is as described in the previous two sections. One has to now match these two solutions by demanding the continuity of δ and $\dot{\delta}$ at the epoch of entering the Hubble radius. After entering the Hubble radius, $\dot{\delta}$ is related to $\boldsymbol{v}$ in linear perturbation theory by

$$\dot{\delta} + \frac{1}{a}\nabla_x \cdot \boldsymbol{v} = 0 . \quad (66)$$

For a spherically symmetric perturbation we then have $v(r) = (-r\bar{\delta}/3)$, where $\bar{\delta}$ is the average value of δ over a sphere of radius r. To get an approximate matching of the solutions, we equate δ and $\dot{\delta}$ obeying equation (66) with δ_{SH} and $\dot{\delta}_{SH}$ determined from equation (65) at the time t_i of entering the Hubble radius. Then one gets, using equation (65),

$$v_i(r_i) = v(r(t_i), t_i) = -\frac{r\bar{\delta}}{3}\bigg|_{t_i} = -\frac{H_i r_i \delta_i}{3}\frac{(2 + y_i)}{(1 + y_i)} = -\frac{\delta_i}{3}\frac{(2 + y_i)}{(1 + y_i)} , \quad (67)$$

since $H_i r_i = 1$. Substituting this v_i in equation (59), we then find the redshift of turnaround in a CDM model to be

$$1 + z_t = \delta_i(1 + z_{eq})E \times \left[\frac{1 - (3y_i/2)(1 + y_i)^{1/2} D_2(y_i)}{1 + (3y_i/2)} + \frac{2 + y_i}{(1 + y_i)^{1/2}} D_2(y_i)\right] . \quad (68)$$

The value of δ_i can be determined from the *COBE* results (Smoot et al. 1992). The *COBE* quadrupole anisotropy $(\Delta T/T)_Q = (0.48 \pm 0.15) \times 10^{-5}$ implies that $\sigma(R) \simeq (R_0/R)^2$ at large scales with $R_0 \simeq (24 \pm 4)\, h^{-1}$ Mpc, if we assume a scale-invariant spectrum (Padmanabhan & Narasimha 1992). For the *maximum* permitted value of $\sigma(R)$, with $R_0 = 28\, h^{-1}$ Mpc, the amplitude of the perturbations on entering the Hubble radius is $\delta_i = (28\, h^{-1}\ \text{Mpc}/3000\, h^{-1}\ \text{Mpc})^2 = 8.7 \times 10^{-5}$.

In Table 3 we have summarized the z_t for various mass scales. We have given both the numerical values of z_t obtained from equation (68) and the results from numerical integration of the exact spherical model. We have taken $1 + z_{eq} = 2.3 \times 10^4(\Omega h^2)$ with $\Omega = 1$ and $h = 0.5$. The results are displayed in Figure 3, which gives a plot of z_t against M. The unbroken line is the result of numerical integration while the dashed line

TABLE 3

TURNAROUND REDSHIFT: CDM MODEL

$(M/M_\odot)$	z_t(exact)	z_t(approx)
9.1×10^9	5.23	4.60
1.1×10^{11}	4.10	3.58
1.3×10^{12}	3.02	2.59
9.9×10^{12}	2.12	1.81
1.1×10^{14}	1.16	0.95

© American Astronomical Society • Provided by the NASA Astrophysics Data System

1993ApJ...417....3P

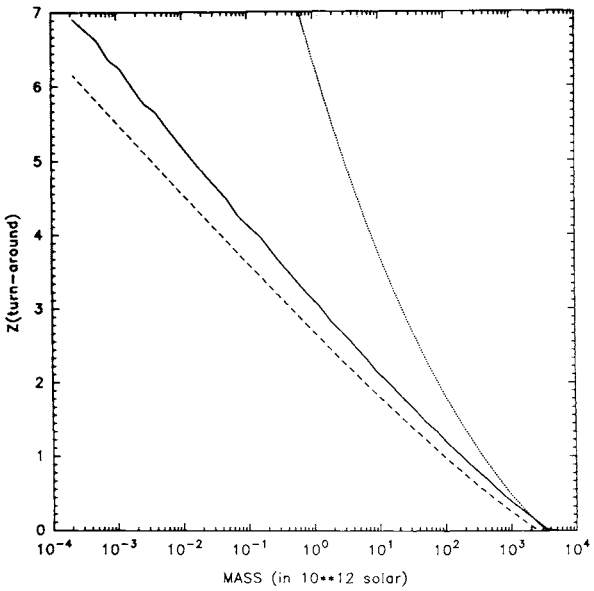

FIG. 3.—Turnaround redshift for different mass scales in a model with initial scale-invariant amplitude. The amplitude of the perturbation at the time of entering the Hubble radius is taken to be $\delta_i = 8.71 \times 10^{-5}$, which is the maximum value allowed by *COBE* measurements of quadrupole anisotropy. The solid curve is based on exact numerical integration; the dashed curve is the analytic approximation. The dotted line shows the result from application of the spherical model to the CDM power spectrum normalized by *COBE* (see text for more details).

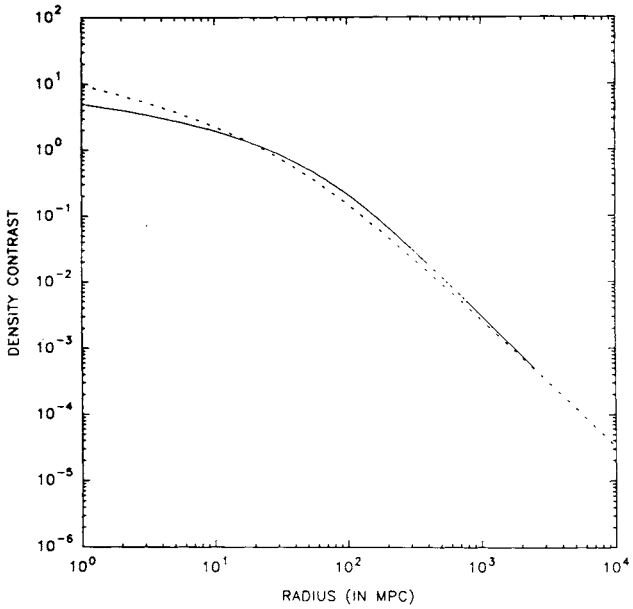

FIG. 4.—Linear density contrast at the present epoch calculated from the analytic approximation (*solid line*). The dotted line is obtained from the CDM spectrum using a spherical window function. Both are normalized using the maximum permitted value of the *COBE* quadrupole anisotropy measurement. We have taken $h = 0.5, \Omega = 1$.

is based on the approximate formula. The difference Δz is only about 0.5 or so even in the extremely nonlinear regime of 10^{10} $M_\odot$. The exact integration suggests that the scale of $M_0 \simeq 4 \times 10^{15}$ $M_\odot$ is at turnaround today. (The approximate formula gives $M_0 \simeq 2.9 \times 10^{15}$ $M_\odot$.)

It is clear from the above analysis that rather large mass scales go nonlinear fairly early. We stress that this phenomenon is purely due to two (rather trivial) factors: (1) We have used for δ_i the *maximum* value permitted by *COBE* quadrupole observations. For this normalization, $\sigma_8 \equiv \sigma(8\ h^{-1}$ Mpc$) \simeq 1.51$, which is about 3 times larger than that of a biased CDM model with $b = 2$. (2) We are computing the reshift z_t *at turnaround* rather than the redshift $z_{\rm coll}$ at "collapse." In a simple spherical model, for example, $(1 + z_{\rm coll}) \cong 0.63(1 + z_m)$.

In order to compare our results with the turnaround redshift computed with the standard CDM power spectrum using the spherical model, we have also plotted the latter in Figure 3 as a dotted line. This redshift $z_{t\rm CDM}$ is obtained using the spherical top-hat model with $v_i = 0$ and is given by $z_{t\rm CDM} \cong (\sigma_0/1.062) - 1$, where σ_0 is the linear density contrast at present computed from the CDM power spectrum with *COBE* maximal normalization. This rises considerably faster at small scales compared with z_t computed by our approximation. This is basically because our $\delta_{\rm lin}$ evaluated at the present epoch is smaller than the corresponding quantity computed from the CDM power spectrum (see below).

The methods developed above can also be used to compute the density contrast $\delta(R)$ at various length scales directly. [This is in contrast to the usual procedure of computing $\delta(R)$ from the Fourier modes δ_k, using a window function.] The results are shown in Figures 4 and 5.

In Figure 4 we have plotted the linear density contrast $\delta_{\rm lin} = -3f$ evaluated at the present epoch (*unbroken line*). For comparison, we have also plotted the $\sigma_{\rm CDM}(R)$ (*dotted line*) evaluated from the CDM spectrum (Peebles 1983, Davis et al. 1985):

$$P(k) = \frac{\alpha k}{(1 + \beta k + \gamma k^{3/2} + \epsilon k^2)^2}\,, \tag{69}$$

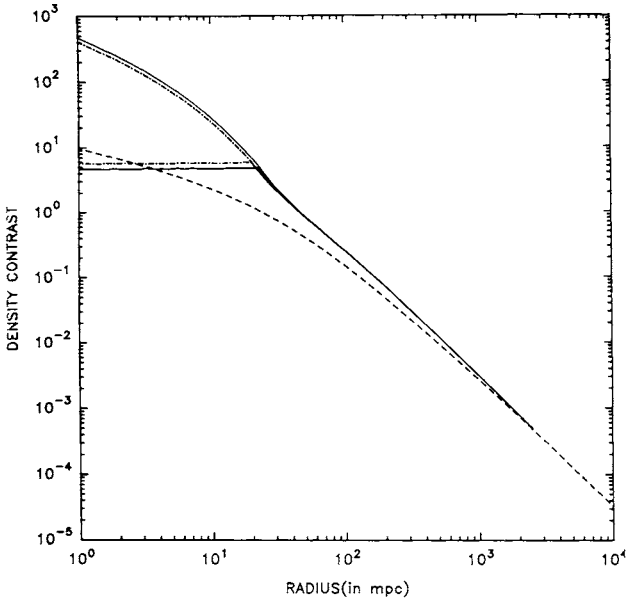

FIG. 5.—Nonlinear density contrast at various comoving scales. The solid line is the result from numerical integration. For scales which have already turned around, we have truncated the density to the value at turnaround. The long-dashed line is the linear density from the CDM model. The dotted line is the result of assuming that the density contrast of structures, which have turned around, grows as a^3. The dot-dash line denotes the corresponding results based on the analytic approximation.

© American Astronomical Society • Provided by the NASA Astrophysics Data System

1993ApJ...417....3P

with $\beta = 1.7(\Omega h^2)^{-1}$ Mpc, $\gamma = 9(\Omega h^2)^{-3/2}$ Mpc$^{3/2}$, and $\epsilon = 1(\Omega h^2)^{-2}$ Mpc^2. The amplitude α is fixed using the maximum permitted value for the *COBE* quadrupole measurement, and a spherical window function is used to get $\sigma_{\rm CDM}(R)$ from $P(k)$. This figure shows that our approximation agrees with the standard $\sigma_{\rm CDM}(R)$ at large scales but underestimates the density contrast at small scales. (This is the reason for the difference between $z_{t\rm CDM}$ and z_t mentioned above in connection with Fig. 3.) We note in passing that $\delta_{\rm lin} = -3f$ computed including the quadratic corrections is in better agreement with $\sigma_{\rm CDM}(R)$ and provides a convenient fitting function for $\sigma_{\rm CDM}(R)$.

In Figure 5 we have plotted the nonlinear density contrast based on exact integration of the equation (*unbroken line*). Obviously, this procedure makes sense only for scales which have not yet turned around. For smaller scales we have extended the unbroken line along the value of density contrast at turnaround (which is about 4.5). An (extreme) alternative hypothesis will be that the density contrast of structures which have turned around grows as a^3. (This is the fully nonlinear limit of "stable clustering"; see Peebles 1980.) The result based on this assumption is shown by a dotted curve. (We would expect the true nonlinear result to lie somewhere between these two extensions.) We have also indicated the corresponding results based on our approximation; see the dash-dot-dash curve. The long-dashed curve is $\sigma_{\rm CDM}(R)$, which is given for comparison.

Finally, we mention the application of our methods to seeded galaxy formation theory like the one based on textures (Turok 1989). In this theory, initial conditions for the evolution of perturbations are most naturally specified in r-space, in contrast to the case of Gaussian random fluctuations which are most easily characterized by giving the power spectrum in k-space. So our formalism is ideally suited to study such seeded theories of structure formation. A collapsing texture gives the matter an initial perturbation which is nearly spherically symmetric and which can be described by (Gooding, Spergel, & Turok 1991) $\delta_i = 0$ and

$$v_i = \begin{cases} -\epsilon[1 - (r_i/a_i\tau_i)] & \text{if } r_i \le t_i\,, \\ 0 & \text{if } r_i \ge a_i T_i\,, \end{cases} \tag{70}$$

where $\tau = \int dt/a(t)$ is the comoving size of the horizon. The fact that $\delta_i = 0$ is related to the isocurvature nature of perturbations seeded by textures. Using these initial conditions in equation (59), we get the turnaround redshift of different spherical shells in texture-seeded collapse to be

$$1 + z_t = E\,\frac{3\epsilon[1 - (r_i/a_i\tau_i)]}{H_i r_i}\,(1 + z_{\rm eq})(1 + y_i)^{1/2} D_2(y_i)\,. \tag{71}$$

Note that the presence of the $(1/r_i)$ term in equation (71) implies that the core region of texture-seeded perturbations collapse much earlier than the outer regions; that is, z_t depends on r_i for any specific perturbed region. Using the results

$$a_i\tau_i = 2^{3/2} H_{\rm eq}^{-1} y_i[(1 + y_i)^{1/2} - 1] \tag{72}$$

and

$$H_i = 2^{-1/2} H_{\rm eq}\,\frac{(1 + y_i)^{1/2}}{y_i^2}\,, \tag{73}$$

we get

$$1 + z_t = 3E\,\frac{1 - q}{2q}\,[\epsilon(1 + z_{\rm eq})]\left[\frac{y_i}{(1 + y_i)^{1/2} - 1}\right] D_2(y_i)\,, \tag{74}$$

where $q = (r_i/a_i\tau_i)$. The value of z_t for a few characteristic masses is shown in Table 4. In preparing this table we have taken $\epsilon = 10^{-4}$, $(1 + z_{\rm eq}) = 2.3\,h^2 \times 10^4$, and $q = 0.5$.

TABLE 4

TURNAROUND REDSHIFT: TEXTURE MODEL

y_i	$\tau_i/2$ (Mpc)	$M/10^{12}\,M_\odot$	z_t
3.98×10^{-3}	1.57×10^{-1}	1.1×10^{-3}	7.59
9.12×10^{-3}	3.6×10^{-1}	1.4×10^{-2}	5.87
1.82×10^{-2}	7.2×10^{-1}	1.1×10^{-1}	4.51
4.16×10^{-2}	1.63	1.3	2.97
9.55×10^{-2}	3.69	1.5×10^{1}	1.63
3.8×10^{-1}	1.38×10^{1}	7.7×10^{2}	0.03

The methods outlined in this paper, therefore, allow us to compute physical parameters in a fairly accurate manner using an analytic approximation. Since this approximation can be applied in a uniform manner in both the linear and nonlinear regimes, we have a fairly simple procedure for handling the growth of inhomogeneities. It should be possible to invert this procedure and obtain the primordial density distribution from the observed mildly nonlinear density contrast in the universe. Suitable modification of these methods will be also of help in studying hybrid models of structure formation (like the ones with hot *and* cold dark matter), especially in the nonlinear regimes. These and related questions are under investigation.

REFERENCES

Buchert, T. 1989, A&A, 223, 9
———. 1992, MNRAS, 254, 729
Davis, M., Efstathiou, G., Frenk, C., & White, S. D. M. 1985, ApJ, 292, 371
Gooding, A. K., Spergel, D. N., & Turok, N. 1991, ApJ, 372, L5
Kolb, E. W., & Turner, M. S. 1990, The Early Universe (New York: Addison-Wesley)
Mészáros, P. 1975, A&A, 38, 5
Padmanabhan, T. 1993, Structure Formation in the Universe (Cambridge: Cambridge Univ. Press)
Padmanabhan, T., & Narasimha, D. 1992, MNRAS, 259, 41P
Peebles, P. J. E. 1980, The Large-Scale Structure of the Universe (Princeton: Princeton Univ. Press)
———. 1983, ApJ, 263, L1
Smoot, G. F., et al. 1992, ApJ, 396, L1
Turok, N. 1989, Phys. Rev. Lett., 63, 2625
Zel'dovich, Ya. B. 1970, A&A, 5, 84

© American Astronomical Society • Provided by the NASA Astrophysics Data System